# Three-state selective population of dressed states via generalized spectral phase-step modulation

Matthias Wollenhaupt,[1] Tim Bayer,[1] Nikolay V. Vitanov,[2,3] and Thomas Baumert[1]

[1]*University of Kassel, Institute of Physics and Center for Interdisciplinary Nanostructure Science and Technology (CINSaT), Heinrich-Plett-Strasse 40, D-34132 Kassel, Germany*

[2]*Department of Physics, Sofia University, James Bourchier 5 Boulevard, 1164 Sofia, Bulgaria*

[3]*Institute of Solid State Physics, Bulgarian Academy of Sciences, Tsarigradsko chaussée 72, 1784 Sofia, Bulgaria*

(Received 17 March 2010; published 26 May 2010)

We present a joint experimental and theoretical study of selective population of dressed states (SPODS) in a three-level system. Control is exerted by shaped intense femtosecond laser pulses generated by a generalized spectral phase-step modulation function. We show that both control parameters (i.e., the phase-step amplitude and position) can be used to switch population among each three dressed states with high selectivity. The dynamics of the system, and hence the resulting photoelectron signal is studied theoretically by analyzing the time evolution of the adiabatic dressed-state energies and populations.

DOI: 10.1103/PhysRevA.81.053422 PACS number(s): 32.80.Qk, 32.80.Rm, 42.50.Md

## I. INTRODUCTION

Quantum control on the ultrafast time scale has opened up new perspectives for the manipulation of light-matter interactions with wide-ranging applications from coherent excitation of model systems to complex interactions with materials [1–12]. In recent time, the focus of quantum control studies has shifted from demonstrations of quantum control to understanding the underlying physical mechanisms of the interaction of shaped femtosecond laser pulses with matter. In particular, control by shaped *intense* laser fields has attracted much interest because nonperturbative light-matter interaction opens novel control pathways which are inaccessible in weak laser fields. A general approach to physically understand control in strong fields has been discussed in terms of selective population of dressed stats (SPODS), which provides a unified picture of distinct control scenarios such as photon locking [13,14], rapid adiabatic passage (RAP) [15], and also stimulated raman adiabatic passage (STIRAP) [16]. SPODS has been demonstrated experimentally, for instance on the Autler-Townes doublet by exerting suboptical cycle control of temporal phase discontinuities employing either double pulses [17] or pulse sequences [18], continually varying phases by chirped laser pulses [19], and combinations thereof [20]. In addition, SPODS by adaptive pulse shaping [21] was reported. Besides two theoretical reports on SPODS on molecules [22,23], these experimental observations have been discussed in the framework of SPODS in an idealized two-state system. Recently, a novel coherent control scenario (robust photon locking [24]) was introduced experimentally making use of adiabatic preparation of a state of maximum coherence followed by photon-locking-type switching. Besides the reported switching mechanism, photoelectrons arising from a third selectively populated dressed state have been observed but not discussed in detail in that article.

In this paper, we generalize the two-level picture to demonstrate SPODS in a three-level system to address the observations of the third dressed state in [24] upon variation of the control parameters in a generalized $\theta$-step spectral phase modulation function. To this end, we investigate the coherent excitation of potassium atoms involving the $4s_{1/2}$ ground state and the two resonantly excited states $4p_{1/2}$ and $4p_{3/2}$. Because the spectral bandwidth (60 meV) of our 30 fs laser pulse is much larger than the fine-structure splitting of both potassium $4p$ states (7.2 meV), the dynamics of both $4p$ states are essentially identical (neglecting the small differences of the respective transition dipole moments) when bandwidth limited pulses are employed. However, making use of shaped pulses, both $4p$ states show different dynamics resulting in selective population of one out of three dressed states.

We start in Sec. II by discussing the properties of the complex temporal pulse shapes due to the generalized $\theta$-step modulation function in some detail. First, we derive some general properties of this type of phase modulation for pulse spectra of arbitrary shape. Subsequently, these properties are exemplified on a Gaussian-shaped pulse spectrum and illustrated for various cases. In Sec. III the experiment recently reported in [24] is briefly summarized. To analyze the underlying physical mechanisms, we discuss the dynamics induced by these *complex* shaped pulses in terms of *adiabatic* dressed states in Sec. IV, based on our previous work on selectivity in a multilevel system via chirped excitation [25].

## II. TEMPORAL PULSE SHAPES FROM GENERALIZED SPECTRAL PHASE-STEP MODULATION

### A. General properties

We start with an initially unmodulated laser pulse

$$E(t) = \mathcal{E}(t)e^{i\omega_0 t}, \tag{1}$$

with a central frequency of $\omega_0$ and a temporal pulse *envelope* $\mathcal{E}(t)$. Fourier transformation of the envelope yields the spectrum $\widetilde{\mathcal{E}}(\omega)$ centered at zero frequency. We study the effect of a generalized spectral phase step defined by the spectral modulation function

$$\begin{aligned}\widetilde{\mathcal{M}}(\omega) &= \exp\left[-i\sigma(\omega - \delta\omega)\frac{\theta}{2}\right] \\ &= \cos\frac{\theta}{2} - i\sigma(\omega - \delta\omega)\sin\frac{\theta}{2},\end{aligned} \tag{2}$$

where $\sigma(\omega - \delta\omega)$ denotes the signum function which takes the values of $\pm 1$ for $\omega \lesseqgtr \delta\omega$. $\widetilde{\mathcal{M}}(\omega)$ is characterized by a phase jump from $-\theta/2$ to $\theta/2$ at a step frequency which

 

is detuned by $\delta\omega$ from the laser central frequency [26–34]. Therefore, the absolute frequency of the step position is $\omega_s = \omega_0 + \delta\omega$. The phase-modulated spectrum reads

$$\widetilde{\mathcal{E}}_{\mathrm{mod}}(\omega) = \widetilde{\mathcal{M}}(\omega)\widetilde{\mathcal{E}}(\omega). \tag{3}$$

Making use of the Fourier convolution theorem [35,36] the modulated temporal electric field is obtained by convolution of the initial unmodulated field $\mathcal{E}(t)$ and the temporal modulation function $\mathcal{M}(t)$

$$\mathcal{E}_{\mathrm{mod}}(t) = \mathcal{M}(t) \circ \mathcal{E}(t). \tag{4}$$

The temporal modulation function $\mathcal{M}(t)$ of the spectral $\theta$-step phase modulation is obtained by inverse Fourier transformation of Eq. (2),

$$\mathcal{M}(t) = \delta(t)\cos\frac{\theta}{2} + \frac{e^{i\,\delta\omega\,t}}{\pi t}\sin\frac{\theta}{2}, \tag{5}$$

where $\delta(t)$ is the Dirac-delta function. Combining Eqs. (4) and (5) yields the modulated temporal electric field

$$\mathcal{E}_{\mathrm{mod}}(t) = \mathcal{E}(t)\cos\frac{\theta}{2} + \mathcal{E}(t) \circ \frac{e^{i\,\delta\omega\,t}}{\pi t}\sin\frac{\theta}{2}. \tag{6}$$

Equation (6) shows that the modulated field $\mathcal{E}_{\mathrm{mod}}(t)$ for any input field $\mathcal{E}(t)$ is a superposition of the unmodulated field and a complex field obtained by convolution with $e^{i\,\delta\omega\,t}/(\pi t)$. By tuning the phase angle $\theta$, we can exert control on their relative contributions via the respective factors $\cos(\theta/2)$ and $\sin(\theta/2)$. The modulated field deviates significantly from the initial unmodulated field if the spectral position of the phase step is not too far detuned from the central frequency (i.e., the phase jump occurs at a spectral position well within the laser spectral bandwidth $\delta\omega < \Delta\omega$). In the temporal wings of the field (i.e., for times much larger than the pulse duration $|t| \gg \Delta t$) the unmodulated contribution $\mathcal{E}(t)\cos\frac{\theta}{2}$ has decayed. In this case, Eq. (5) reveals that the modulated field rises and decays proportional to

$$\mathcal{E}_{\mathrm{mod}}(t) \propto \frac{1}{t}. \tag{7}$$

Equations (5) and (6) also imply that in the temporal wings of the modulated field the instantaneous detuning $\Delta(t)$ – defined as the time derivative of the temporal phase $\zeta(t) = \arg\mathcal{E}_{\mathrm{mod}}(t)$ of the modulated field, $\Delta(t) = \dot{\zeta}(t)$ – converges to the detuning of the $\theta$-step position with respect to the central laser frequency $\delta\omega$

$$\Delta(t) \underset{t\to\pm\infty}{\longrightarrow} \delta\omega. \tag{8}$$

Summing up, Eqs. (7) and (8) show that for any shape of the pulse spectrum the temporal pulse starts and ends very smoothly with constant detuning from the central laser frequency determined by the spectral position of the $\theta$ step.

For the important case when the $\theta$ phase jump occurs at the central laser frequency (i.e., $\delta\omega = 0$) Eq. (6) reduces to

$$\mathcal{E}_{\mathrm{mod}}(t) = \mathcal{E}(t)\cos\frac{\theta}{2} - \hat{\mathcal{E}}(t)\sin\frac{\theta}{2}, \tag{9}$$

where $\hat{\mathcal{E}}(t)$ describes the Hilbert transform of $\mathcal{E}(t)$. In writing Eq. (9) we made use of the fact that convolution with $-1/(\pi t)$ yields the Hilbert transform [35]

$$\mathcal{E}(t) \circ \frac{1}{\pi t} = -\frac{1}{\pi}\mathrm{P}\int_{-\infty}^{\infty}\frac{\mathcal{E}(\tau)}{\tau - t}\,d\tau = -\hat{\mathcal{E}}(t), \tag{10}$$

where P denotes the Cauchy principal value. For $\delta\omega = 0$ the spectral phase modulation function is symmetrical with respect to the pulse spectrum for all values of $\theta$, and therefore this type of modulation delivers a real-valued modulated temporal pulse envelope $\mathcal{E}_{\mathrm{mod}}(t)$ in accordance with Eq. (9) (provided the unmodulated field envelope $\mathcal{E}(t)$ was real-valued, i.e., the modulus of the spectrum $|\widetilde{\mathcal{E}}(\omega)|$ is of even symmetry). As a consequence, the temporal phase of the envelope is zero (apart from $\pi$ phase jumps reflecting zero crossings of the envelope), implying a constant instantaneous frequency and detuning, respectively. Equation (9) shows that resonant $\theta$-step modulation of an arbitrary input field $\mathcal{E}(t)$ delivers a modulated field being a superposition of the unmodulated field and its Hilbert transform where the phase angle $\theta$ controls the weights of both interfering contributions. A phase angle of $\theta = 2n\pi$ leaves the field obviously unmodulated, whereas for $\theta = (2n+1)\pi$ the modulated field is the Hilbert transform $\hat{\mathcal{E}}(t)$ of the unmodulated field. The superposition character of the modulated field is illustrated in Fig. 1 for step amplitudes of $\theta = \pi/2$, $\pi$, and $3\pi/2$. Note that a temporal phase jump of $\pi$ occurs due to a change of sign of the envelope when $\cos(\theta/2)\,\mathcal{E}(t)$ and $\sin(\theta/2)\,\hat{\mathcal{E}}(t)$ cancel each other. Therefore, the choice of $\theta$ controls—besides the pulse shape—also the location of the temporal phase jump.

### B. Gaussian pulses

For practical applications—such as analytical models or numerical simulations of the dynamics induced by a modulated pulse—we discuss the effect of $\theta$-step spectral phase modulation for a Gaussian shaped pulse envelope as the most relevant example. Analytic solutions for this special pulse shape are given for the general $\theta$-step modulation at an arbitrary spectral

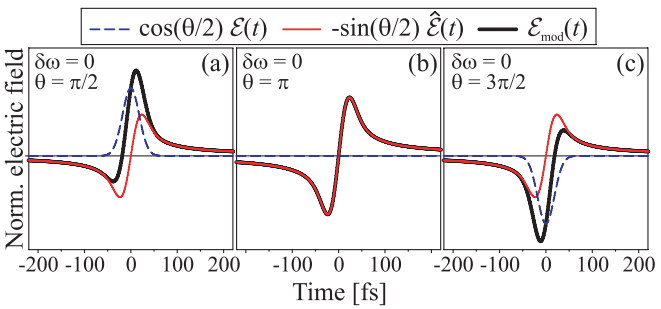


FIG. 1. (Color online) Decomposition of the temporal electric field envelope $\mathcal{E}_{\mathrm{mod}}(t)$ of (a) a $\theta = \pi/2$, (b) $\pi$, and (c) $3\pi/2$-step phase-modulated Gaussian input pulse at the central laser frequency (black bold line) into the unmodulated contribution $\cos(\theta/2)\mathcal{E}(t)$ (blue dashed line) and the contribution of its Hilbert transform $-\sin(\theta/2)\hat{\mathcal{E}}(t)$ (red thin line) according to Eq. (9). Note that a temporal phase jump of $\pi$ occurs at the moment when $\cos(\theta/2)\mathcal{E}(t)$ and $\sin(\theta/2)\hat{\mathcal{E}}(t)$ cancel each other.

detuning $\delta\omega$. The Gaussian temporal electrical field envelope is given by

$$\mathcal{E}^G(t) = \varepsilon_t \, e^{-\ln 4 \left(\frac{t}{\Delta t}\right)^2}, \tag{11}$$

where $\Delta t$ describes the full width at half maximum (FWHM) of the temporal intensity profile, and the electrical field strength

$$\varepsilon_t = \mathcal{E}_0 \sqrt[4]{\frac{2 \ln 4}{\pi \, \Delta t^2}}, \tag{12}$$

is so chosen as to normalize the field to a pulse energy proportional to

$$\int_{-\infty}^{\infty} [\mathcal{E}^G(t)]^2 \, dt = \mathcal{E}_0^2. \tag{13}$$

By modulating the Gaussian spectrum

$$\widetilde{\mathcal{E}}^G(\omega) = \varepsilon_\omega \, e^{-\ln 4 \left(\frac{\omega}{\Delta\omega}\right)^2}, \tag{14}$$

having a spectral intensity FWHM of $\Delta\omega = (2 \ln 4)/\Delta t$ and a normalized field strength of

$$\varepsilon_\omega = \mathcal{E}_0 \sqrt[4]{\frac{\pi \, \Delta t^2}{\ln 2}}, \tag{15}$$

with the spectral modulation function described in Eq. (2) we obtain the modulated temporal field as

$$\mathcal{E}^G_{\rm mod}(t) = \mathcal{E}^G(t) \left\{ \cos\frac{\theta}{2} + \sin\frac{\theta}{2} \, \mathrm{Erfi}\left[ \sqrt{\ln 4} \left( \frac{t}{\Delta t} + i \, \frac{\delta\omega}{\Delta\omega} \right) \right] \right\}, \tag{16}$$

where $\mathrm{Erfi}(z)$ denotes the complex error function. To yield a physically more transparent description of the modulated pulse shape described in Eq. (16), we approximate

$$\mathrm{Erfi}(x + iy) \approx \exp(-y^2 + 2\,i\,x\,y)\,\mathrm{Erfi}(x), \tag{17}$$

for $x \gg y$. In the temporal wings [when the unmodulated contribution proportional to $\cos(\theta/2)$ has decayed] we obtain for $t/\Delta t \gg \delta\omega/\Delta\omega$

$$\mathcal{E}^G_{\rm mod}(t) \approx \mathcal{E}^G(t)\,\mathrm{Erfi}\left( \frac{\sqrt{\ln 4}\, t}{\Delta t} \right) \times \; e^{-\ln 4 \left(\frac{\delta\omega}{\Delta\omega}\right)^2} \, e^{i\,\delta\omega\, t} \; \sin\frac{\theta}{2}. \tag{18}$$

The phase factor $\exp(i\,\delta\omega\,t)$ in the lower part of Eq. (18) leads to the asymptotic constant detuning of $\Delta(t) = \delta\omega$. Further simplification of the *upper* part of Eq. (18) by approximating the asymptote of Dawson's function $\exp(-y^2)\mathrm{Erfi}(y)$ by $1/(\sqrt{\pi}\,y)$ yields

$$\mathcal{E}^G_{\rm mod}(t) \underset{t\to\pm\infty}{\sim} \frac{\widetilde{\mathcal{E}}(\delta\omega)}{2\sqrt{\pi}} \, \frac{e^{i\,\delta\omega\,t}}{t} \sin\frac{\theta}{2}, \tag{19}$$

revealing both relevant properties of the modulated pulse: (i) the decay of the modulated pulse envelope proportional to $1/t$ and (ii) the asymptotic detuning of $\Delta(t) = \delta\omega$, both of which are relevant to the experiment and illustrated in Fig. 2.

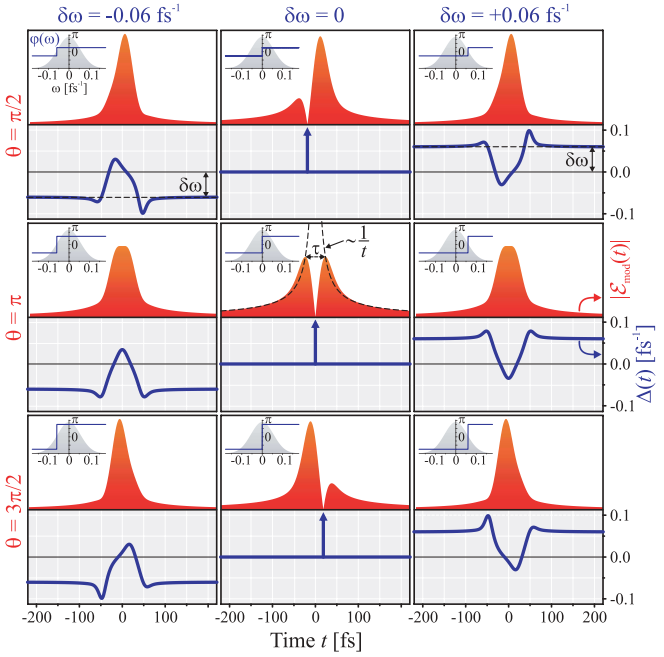


FIG. 2. (Color online) Modulated pulse shapes (envelope $|\mathcal{E}_{\rm mod}(t)|$ red shaded and instantaneous detuning $\Delta(t)$ bold blue line, right scale) for various values of the phase-step amplitude and spectral detuning from the laser central frequency. The unmodulated Gaussian field has a FWHM of $\Delta t = 30$ fs. In the temporal wings, the envelope rises and decays as $1/|t|$ and the instantaneous detuning converges to the spectral detuning of the phase-step $\delta\omega$. The insets show the corresponding spectral phase (thin blue line) and amplitude (gray shaded background). The central panel shows the well-known $\pi$ jump at central frequency ($\theta = \pi$ and $\delta\omega = 0$) with a subpulse separation of $\tau \approx 1.57\,\Delta t$.

For the $\theta$-step spectral modulation of a Gaussian laser pulse at the central frequency (i.e., $\delta\omega = 0$) Eq. (16) reduces to

$$\mathcal{E}^G_{\rm mod}(t) = \mathcal{E}^G(t) \left[ \cos\frac{\theta}{2} + \sin\frac{\theta}{2} \, \mathrm{Erfi}\left( \frac{\sqrt{\ln 4}\, t}{\Delta t} \right) \right], \tag{20}$$

which is a special case of Eq. (9) since

$$\hat{\mathcal{E}}^G(t) = -\mathcal{E}^G(t)\,\mathrm{Erfi}\left( \frac{\sqrt{\ln 4}\, t}{\Delta t} \right), \tag{21}$$

is the Hilbert transform of the unmodulated Gaussian $\mathcal{E}^G(t)$.

Figure 2 illustrates modulated Gaussian electric fields, decomposed into their envelope $|\mathcal{E}_{\rm mod}(t)|$ (red shaded) and instantaneous detuning $\Delta(t)$ (bold blue lines), for various combinations of the modulation parameters $\theta$ and $\delta\omega$. Note that the middle *column* of the $3 \times 3$ matrix of figures corresponds to Fig. 1. The center of the matrix displays the well-known $\pi$ jump at central frequency [$\theta = \pi$ and $\delta\omega = 0$, cf. Fig. 1(b)], being the Hilbert transform of the Gaussian input field. This field has a double-pulse structure with a temporal separation of about $\tau \approx 1.57\,\Delta t$ and an intensity FWHM of each subpulse of approximately $1.04\,\Delta t$. The change of sign of the envelope is responsible for the phase jump of $\pi$ in between both subpulses. As a consequence, the instantaneous detuning exhibits a delta peak at $t = 0$. Since both subpulses have the same pulse area, the total pulse

area is zero. This is an exceptional realization of a zero-area pulse [37] because it is generated by spectral phase modulation, which leaves the modulus of the pulse area $\Theta^{\infty}$, in general, unchanged

$$\Theta^{\infty}_{\mathrm{mod}} = \int_{-\infty}^{\infty} \mathcal{E}_{\mathrm{mod}}(t)\,dt = \widetilde{\mathcal{E}}_{\mathrm{mod}}(0) = \widetilde{\mathcal{M}}(0)\widetilde{\mathcal{E}}(0)$$
$$= \widetilde{\mathcal{M}}(0)\int_{-\infty}^{\infty} \mathcal{E}(t)\,dt = \widetilde{\mathcal{M}}(0)\Theta^{\infty}. \qquad (22)$$

The dashed black line proportional to $1/t$ indicates the hyperbolic rise and decay of the field at early and late times [cf. Eqs. (7) and (19)]. Variation of $\theta$ to either $\pi/2$ or $3\pi/2$ [cf. Figs. 1(a) and 1(c)] leads to a superposition of the unmodulated field and its Hilbert transform, shifting the zero of the envelope to early and late times, respectively. For $\theta = \pi/2$ this results in the formation of a weak prepulse followed by a strong postpulse, whereas for $\theta = 3\pi/2$ the result is a time-reversed copy (i.e., a strong prepulse followed by a weak postpulse). However, since in both cases the spectral phase function is still antisymmetric with respect to the laser central frequency, the modulated *temporal* field envelopes $\mathcal{E}_{\mathrm{mod}}(t)$ are real valued [38] and no change of the instantaneous detuning occurs (apart from the delta peaks due to the $\pi$ jump in the temporal phase). It was shown [19,38] that in two-level systems real-valued resonant pulses are incapable of exerting control on dressed-state populations. In general, however, in multilevel systems there is no distinct single resonance and hence "real-valued pulses" are no longer well defined. As a consequence, antisymmetric spectral phase functions will generally affect the dressed-state populations. Manipulation of the instantaneous detuning $\Delta(t)$ is achieved in particular by variation of the step detuning $\delta\omega$. Most importantly, $\delta\omega$ defines the asymptotic value of $\Delta(t)$ in the wings of the pulse [cf. Eqs. (8) and (19)] as can be seen throughout the left and right columns where $\delta\omega \lesseqgtr 0$. Around $t = 0$ the two subpulses merge to one pulse, and consequently, the $\pi$ jump of the temporal phase is blurred, yielding a strong nonlinear variation of the instantaneous detuning. For $\theta = \pi$ the field is symmetric in time, whereas the choice of $\theta = \pi/2$ or $3\pi/2$ introduces a temporal asymmetry to both the field envelope and detuning. Since changing the step amplitude from $\pi/2$ to $3\pi/2$ (equivalent to $-\pi/2$) amounts to phase conjugation of the pulse spectrum [i.e., $\widetilde{\mathcal{E}}_{\mathrm{mod}}(\omega) \to \widetilde{\mathcal{E}}^{*}_{\mathrm{mod}}(\omega)$] the corresponding temporal field is likewise phase conjugated and additionally time reversed: $\mathcal{E}_{\mathrm{mod}}(t) \to \mathcal{E}^{*}_{\mathrm{mod}}(-t)$. As a consequence, both the envelope and the instantaneous detuning are reversed in time [i.e., $|\mathcal{E}_{\mathrm{mod}}(t)| \to |\mathcal{E}_{\mathrm{mod}}(-t)|$ and $\Delta(t) \to \Delta(-t)$] since the time derivative of the conjugated and time reversed temporal phase is $d/dt[-\zeta(-t)] = \dot{\zeta}(-t) = \Delta(-t)$. On the other hand, changing the sign of the step detuning $\delta\omega \to -\delta\omega$ corresponds to a reversal of the spectral phase-modulation function with respect to *both* axes. Taking into account the symmetry of the pulse spectrum, this implies phase conjugation and frequency reversal of the spectrum, $\widetilde{\mathcal{E}}_{\mathrm{mod}}(\omega) \to \widetilde{\mathcal{E}}^{*}_{\mathrm{mod}}(-\omega)$, and hence phase conjugation of the modulated *temporal* field: $\mathcal{E}_{\mathrm{mod}}(t) \to \mathcal{E}^{*}_{\mathrm{mod}}(t)$. This entails that the instantaneous detuning is inverted, $\Delta(t) \to -\Delta(t)$, while the envelope of the temporal field remains unaltered.

In summary, changing the sign of $\theta$ leads to time reversal of the modulated temporal field (i.e., of both the envelope and the instantaneous detuning) whereas changing the sign of $\delta\omega$ mirrors only the detuning with respect to the $t$ axis. In the case of $\theta = \pi$, the modulated spectrum is unaltered upon phase conjugation implying *gerade* symmetry of the temporal field in terms of envelope and detuning as seen in the middle row of Fig. 2.

## III. EXPERIMENT

The experimental setup for strong-field excitation of a three-level system in potassium atoms is shown in Fig. 3. Intense 795 nm, 30 fs FWHM laser pulses provided by an amplified 1 kHz Ti:sapphire laser system were phase modulated by a home-built pulse shaper [39,40], applying a $\theta$-step phase mask, Eq. (2). The shaped output pulses were attenuated to pulse energies of 0.6–1.4 $\mu$J and focused by a 300 mm lens into a potassium atomic beam. Photoelectrons released in a resonance-enhanced multiphoton ionization (REMPI) process during the laser-atom interaction were detected by an energy-calibrated magnetic bottle time-of-flight spectrometer with a kinetic-energy resolution of 15 meV at 0.5 eV. Prior to the experiments we performed an *in situ* compensation of the residual spectral phase of the input pulse in the interaction region of the photoelectron spectrometer. To this end, we parameterized the compensation phase in terms of

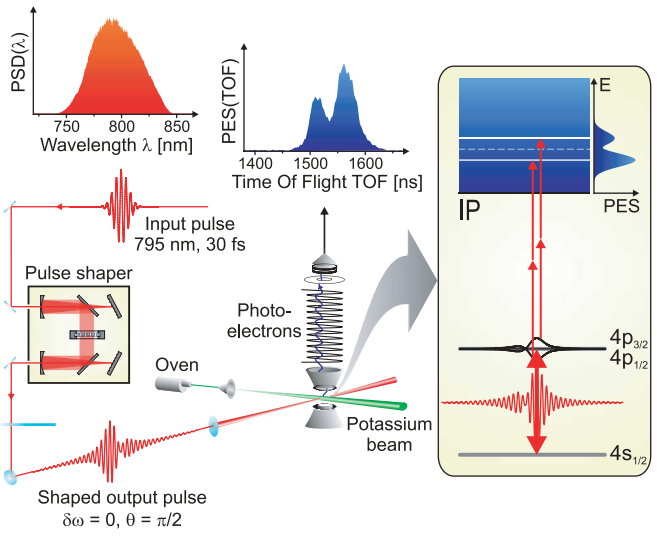


FIG. 3. (Color online) Schematic of the experimental setup. Ultrashort infrared laser pulses, phase modulated by a Fourier transform pulse shaper, are focused into a vacuum chamber to intersect a potassium atomic beam. Photelectrons released during the light-atom interaction are detected by a time-of-flight magnetic bottle spectrometer. The right frame displays the excitation and ionization scheme of potassium atoms interacting with the shaped light field: The transitions $4p_{1/2,3/2} \leftarrow 4s_{1/2}$ (bold gray) are driven strongly near resonance, giving rise to three dressed states (black), the energies and populations of which are probed via two-photon ionization by the most intense part of the excitation pulse.

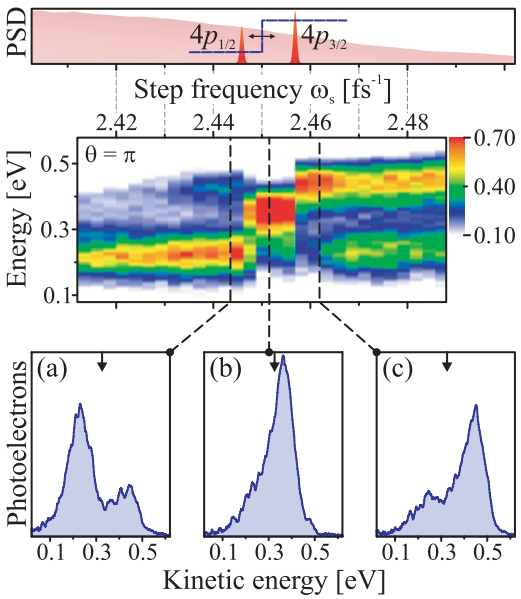


FIG. 4. (Color online) Measured photoelectron spectra for a fixed step amplitude of $\theta = \pi$ and the spectral step position $\omega_s$ scanned across the two potassium fine-structure resonances $4p_{1/2}$ and $4p_{3/2}$. Both resonances (red peaks in the top frame) are much narrower then the spectral resolution of our pulse shaper of about 1 nm and lie in the blue wing of the laser power spectral density (PSD; light red shaded background in the top frame). (a) and (c) show sections through the scan slightly below and slightly above both resonances, respectively. The arrows mark the bare state (i.e., weak-field position of the photoelectron peak). In (a) predominantly low-energetic photoelectrons are detected, indicating selective population of the lower dressed state, whereas in (c) the high-energetic photoelectrons are promoted, revealing selective population of the upper dressed state. Selective population of the third, intermediate dressed state is realized when the phase step occurs in between the two resonances as indicated by the photoelectron spectrum in (b) having a sharp and pronounced maximum at medium kinetic energies.

a fifth-order Taylor polynomial and employed an adaptive optimization procedure to maximize the photoelectron yield from multiphoton ionization of xenon atoms. The optimal compensation phase was additionally applied to the pulse shaper throughout the following experiments to ensure a flat spectral phase of the input pulse.

In a first experiment we studied energy-resolved photoelectron spectra as a function of the absolute step frequency $\omega_s$ by sweeping a $\theta = \pi$ step across the laser spectrum. Figure 4 shows the photoelectron spectra obtained in the vicinity of the two potassium fine-structure resonances $4p_{1/2}$ and $4p_{3/2}$. The experimental results show that—in addition to the common Autler-Townes doublet—a third dressed state is observed in the photoelectron spectra. By suitable choice of $\omega_s$, we were able to exert efficient control on three distinct photoelectron spectra each mapping the selective population of one out of three dressed states. In the second experiment we chose two distinct step frequencies (one slightly below, the other one slightly above both resonances) to be kept fixed while the step amplitude $\theta$ was varied. Resulting photoelectron spectra presented in Fig. 7 demonstrate that the step amplitude $\theta$ is an efficient control parameter as well.

## IV. PHYSICAL MECHANISM

### A. The physical system

The physical mechanism of the potassium experiment involves three atomic states: $4s_{1/2}$, $4p_{1/2}$, and $4p_{3/2}$. The laser-excited system is described by the Hamiltonian [15,41,42]

$$H = \hbar \begin{bmatrix} \omega_1 & \frac{1}{2}\Omega_{12} & \frac{1}{2}\Omega_{13} \\ \frac{1}{2}\Omega_{12}^* & \omega_2 & 0 \\ \frac{1}{2}\Omega_{13}^* & 0 & \omega_3 \end{bmatrix}. \tag{23}$$

The excitation pulse couples both transitions $4p_{1/2} \leftarrow 4s_{1/2}$ and $4p_{3/2} \leftarrow 4s_{1/2}$. The control parameters are the amplitude $\theta$ of the phase step and its position $\omega_s$ in the pulse spectrum.

The central laser frequency is $\omega_0 = 2.3844$ fs$^{-1}$ ($\lambda_0 = 790$ nm) and the characteristic width of the spectrum is $\Delta\omega = 0.092$ fs$^{-1}$, which corresponds to an intensity FWHM of $\Delta t = 30$ fs. Note that we abbreviate the unit of angular frequencies rad/fs by fs$^{-1}$. For simplicity, we assume that the dipole moments of the transitions $4p_{1/2} \leftarrow 4s_{1/2}$ and $4p_{3/2} \leftarrow 4s_{1/2}$ are equal (the actual small difference of 3.4 a.u. to 4.8 a.u. [43] does not alter the picture in the present context). The eigenfrequencies of the three states are $\omega_1 = 0$ ($4s_{1/2}$), $\omega_2 = 2.446$ fs$^{-1}$ ($4p_{1/2}$), and $\omega_3 = 2.457$ fs$^{-1}$ ($4p_{3/2}$).

The phase step in the Fourier transform produces a complex Rabi frequency $\Omega(t) = |\Omega(t)|\, e^{i \arg \Omega(t)}$, with the argument being the *total* temporal phase $\arg \Omega(t) = \omega_0 t + \zeta(t)$. After an appropriate phase transformation of the probability amplitude of state $4s_{1/2}$, $c_1(t) = b_1(t) e^{i[\omega_0 t + \zeta(t)]}$, the time derivative of the total temporal phase [being the instantaneous frequency $\omega_0 + \Delta(t)$] translates into a time-dependent energy of state $4s_{1/2}$,

$$H(t) = \hbar \begin{bmatrix} \omega_0 + \Delta(t) & \frac{1}{2}|\Omega(t)| & \frac{1}{2}|\Omega(t)| \\ \frac{1}{2}|\Omega(t)| & \omega_2 & 0 \\ \frac{1}{2}|\Omega(t)| & 0 & \omega_3 \end{bmatrix}. \tag{24}$$

This representation of the Hamiltonian is used in the dressed-state analysis in the following. The corresponding state vectors will be denoted by $|1\rangle$, $|2\rangle$, and $|3\rangle$, respectively. The above phase transformation amounts to a reference frame rotating with the instantaneous frequency of the driving laser field.

In accordance with Eq. (8), the phase-step chirped energy of state $|1\rangle$ tends asymptotically toward the absolute position of the phase step $\omega_s$ at early and late times

$$\omega_0 + \Delta(t) \underset{t \to \pm\infty}{\longrightarrow} \omega_s. \tag{25}$$

This property is essential for the analysis in the following. The experimental conditions are also such that the pulsed interactions in the two transitions have large pulse areas $\Theta^\infty$ [here the pulse area is defined by the integral over the Rabi frequency implying multiplication of Eq. (22) with the dipole moment]. The Autler-Townes splitting of 257 meV $\approx 0.39$ fs$^{-1}$ indicates a pulse area of about $\Theta^\infty = 6\pi$ for a Gaussian pulse. This implies that the evolution is *nearly adiabatic* (i.e., the adiabatic condition) [15,41]

$$\left| \Delta \frac{d}{dt}|\Omega| - |\Omega| \frac{d}{dt}\Delta \right| \ll 2(\Delta^2 + |\Omega|^2)^{3/2}, \tag{26}$$

is essentially fulfilled. The physical mechanism is therefore the one of adiabatic dressed-state evolution.

### B. Dressed-state picture for $\pi$ phase step

The photoelectron (PE) signal is explained most naturally in the dressed-state picture by examining the eigenstates (referred to as adiabatic or dressed states) of the Hamiltonian (24). There are three such dressed states, as displayed in Fig. 5. The spectral phase step induces a time-dependent chirp in the energy of state $|1\rangle$, depicted by the gray solid-dotted line, which tends asymptotically to $\omega_s$, Eq. (25). Because this state is the only one populated initially, the value of $\omega_s$ determines which dressed state is initially populated; the (adiabatic) evolution then proceeds through this state, which in turn determines the kinetic energy of the detected photoelectrons. We have three distinct cases.

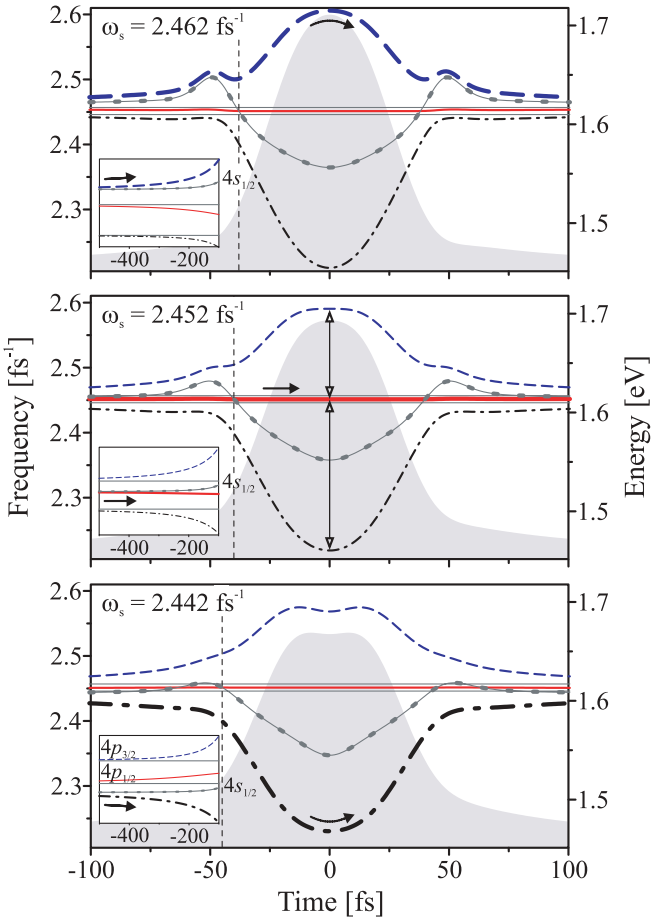


FIG. 5. (Color online) Dressed-state energies of potassium atoms for three values of the phase step position $\omega_s = 2.442$, 2.452 and 2.462 fs$^{-1}$. The other parameters are $\Omega_0 = 0.39$ fs$^{-1}$, $\Delta\omega = 0.092$ fs$^{-1}$, and $\theta = \pi$. Since all three step frequencies are larger than the laser central frequency, the modulated fields correspond to the middle right frame of Fig. 2. The black dashed-dotted, the red solid, and the blue-dashed curves show the dressed-state energies, whereas the thin gray solid lines depict the bare state (diabatic) energies. In particular, the gray solid-*dotted* curve depicts the phase-step chirped energy of state $|1\rangle$, which is the initially populated bare state. The Rabi frequency is depicted as the gray shaded background. Vertical arrows in the middle frame exemplify the energy separation of the dressed states during the most intense part of the pulse. This splitting is generally mapped into the photoelectron spectrum since most of the photoelectrons are released during this time window.

(1) $\omega_2 < \omega_3 < \omega_s$. The energy of state $|1\rangle$ is initially *above* the energies of states $|2\rangle$ and $|3\rangle$ (Fig. 5, top frame, $\omega_s = 2.462$ fs$^{-1}$). Consequently, the evolution proceeds via the *highest* dressed state and the resulting PE's have the highest kinetic energy, as seen in Fig. 4 for $\omega_s \approx 2.462$ fs$^{-1}$. This observation is supported by the calculated dressed-state populations shown in the top frame of Fig. 6, which indicate very efficient population of the upper dressed state throughout the most intense part of the pulse. In fact, some population escapes to the lower dressed state because the avoided crossing around $t = -38$ fs in Fig. 5 (marked by the vertical dashed line) is relatively narrow since the intensity is just beginning to increase and the evolution is not sufficiently adiabatic yet. Because the fine-structure splitting of the atomic bare states $4p_{1/2}$ and $4p_{3/2}$ is much smaller than both the peak Rabi frequency and the phase-step-induced shift $\Delta(t)$ (cf. Fig. 5), these two states are nearly at two-photon resonance [15] (i.e., $4p_{1/2} \leftrightarrow 4s_{1/2} \leftrightarrow 4p_{3/2}$). As a consequence—and also depicted in the plot of the time evolution of the bare state populations shown in the inset to the upper panel of Fig. 6—the atom evolves like a three-state system consisting of a ground state coupled to two *degenerate* excited states. Because such a system is equivalent to an effective two-state system [44] the intermediate dressed state is (almost) dark (i.e., decoupled from the other dressed states) implying that it is excluded from the population redistribution. Therefore the population that escapes from the initially populated upper dressed state flows into the lowest dressed state, bypassing the intermediate (nearly dark) dressed state as evident from Fig. 6, top frame. In the experimental results, Fig. 4, the population of the lower dressed state is indicated by the low-energy PE signal for step frequencies $\omega_s > 2.465$ fs$^{-1}$.

(2) $\omega_2 < \omega_s < \omega_3$. The energy of state $|1\rangle$ is initially *between* the energies of states $|2\rangle$ and $|3\rangle$ (Fig. 5, middle frame, $\omega_s = 2.452$ fs$^{-1}$). In this case the evolution proceeds via the *intermediate* dressed state and the PE's have a medium kinetic energy, as seen very distinctively in Fig. 4 for $\omega_s \approx 2.452$ fs$^{-1}$. As we pointed out above, the intermediate dressed state is almost dark and hence it is nearly decoupled from the other two dressed states. Consequently, only marginal population escapes to the other dressed states, which is evident from the calculated dressed-state populations (see Fig. 6, middle frame) and, in particular, from the absence of low-energy and high-energy PE's in the PE spectrum Fig. 4(b). Moreover, the avoided crossing at $t = -38$ fs is now wider (due to the temporal broadening of the pulse), and does not influence significantly the population distribution. These PE spectra are particularly remarkable because they show a single peak while the potassium atoms are excited (almost) resonantly with an intense femtosecond laser pulse capable of producing an Autler-Townes splitting of about 250 meV.

(3) $\omega_s < \omega_2 < \omega_3$. The energy of state $|1\rangle$ is initially *below* the energies of states $|2\rangle$ and $|3\rangle$ (Fig. 5, bottom frame, $\omega_s = 2.442$ fs$^{-1}$). The evolution proceeds via the *lowest* dressed state and the PE's have the lowest kinetic energy, as seen in Fig. 4 for $\omega_s \approx 2.442$ fs$^{-1}$. The avoided crossing at $t = -45$ fs is wider than for $\omega_s = 2.462$ fs$^{-1}$ and hence,

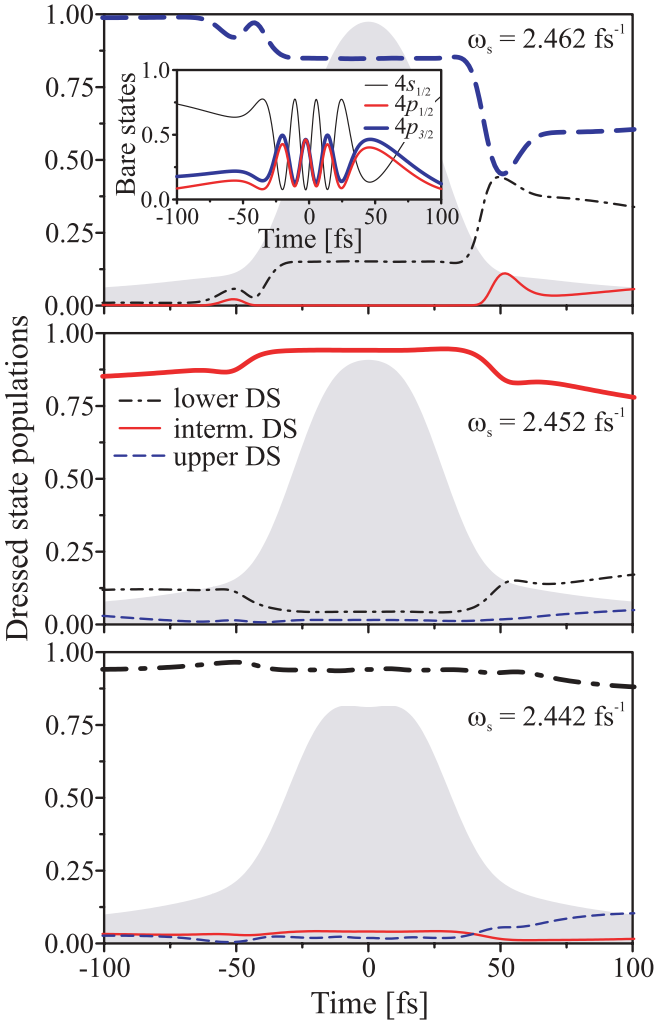


FIG. 6. (Color online) Dressed State (DS) populations for a step amplitude of $\theta = \pi$ and three values of the phase-step position $\omega_s = 2.442, 2.452$, and $2.462\ \mathrm{fs}^{-1}$, corresponding to the scenarios displayed in Fig. 5. The inset to the upper panel shows the time evolution of the bare state populations.

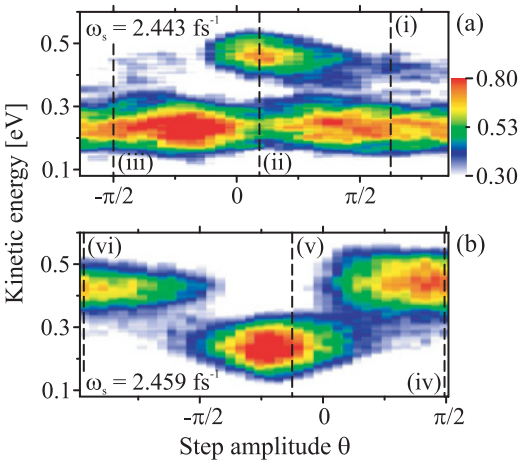


FIG. 7. (Color online) Experimental PE spectra for fixed step positions of (a) $\omega_s = 2.443\ \mathrm{fs}^{-1}$ and (b) $\omega_s = 2.459\ \mathrm{fs}^{-1}$ and various step amplitudes $\theta$. These results show that once a certain energy channel is selected via the phase-step frequency (at $\theta = \pi$, cf. Fig. 4) the target channel can be switched efficiently via the step amplitude, reminiscent of a toggle switch.

the escaped population to the other dressed states is less. As a result, the lower dressed state is selectively populated throughout the pulse, as confirmed by the simulation shown in the bottom frame of Fig. 6 and evident from the low-energy PE's observed in the experiment [cf. Fig. 4(a)].

The conclusion is that the *position* $\omega_s$ of the $\pi$ step can be exploited as an efficient *control parameter* for the population of a particular dressed state. We point out that the sharp edges in the PE spectrum in Fig. 4 indicate highly adiabatic evolution: the value of the phase-step position $\omega_s$ determines unambiguously (except at the edges, i.e., resonances $\omega_s = \omega_2$ or $\omega_3$) which dressed state is populated initially, and since the evolution is highly adiabatic, no significant population escapes to the initially unpopulated dressed states (except for some population in the case $\omega_s = 2.462\ \mathrm{fs}^{-1}$). Another curious observation from Fig. 4 is that the central PE peak, situated at medium kinetic energies, is closer to the high-energy peak than to the low-energy one. This feature is explained by looking again at the dressed-state energies (black dashed-dotted, red solid, and blue dashed curves) in Fig. 5: The intermediate dressed-state energy is closer to the upper dressed-state energy than to the lower one, as indicated by the vertical arrows in the middle frame of Fig. 5. This observation demonstrates again that the PE spectra map the energies and populations of the dressed states rather than those of the bare states [18].

### C. Variable phase-step amplitude

Figure 7 shows the experimental PE spectra for varying phase-step amplitude $\theta$ at two different step positions: one for $\omega_s = 2.443\ \mathrm{fs}^{-1}$ [$\omega_s < \omega_2 < \omega_3$, Fig. 7(a)] and another for $\omega_s = 2.459\ \mathrm{fs}^{-1}$ [$\omega_2 < \omega_3 < \omega_s$, Fig. 7(b)]. This figure demonstrates that the *amplitude* of the phase step can be used as a control parameter as well, similarly to the *position* of the phase-step discussed previously.

The observed features in the PE spectrum are explained by examining the dressed-state energies. Figure 8 presents the dressed-state picture for a fixed position of the phase step, $\omega_s = 2.443\ \mathrm{fs}^{-1}$, and for three values of the phase-step amplitude: (i) $\theta = 3\pi/4$, (ii) $\theta = \pi/6$, and (iii) $\theta = -\pi/2$, which correspond to three distinct regions in Fig. 7(a). For this value of $\omega_s$, as discussed in regard to Fig. 5, it is the *lowest* dressed state that is populated for amplitude $\theta = \pi$. For other values of $\theta$, the temporal symmetry of the dressed-state picture of Fig. 5 is distorted, which leads to the emergence of *avoided crossings*; the latter may alter the evolution path. In the *upper* frame of Fig. 8 (for $\theta = 3\pi/4$) an avoided crossing is identified around $t = -40$ fs. This avoided crossing, however, is too broad and hence it does not alter the course of the evolution which proceeds via the lowest dressed state and results in low-energy PE's. In the *middle* frame of Fig. 8 (for $\theta = \pi/6$), the avoided crossing occurs again around $t = -40$ fs but turns out to be narrower, so that some population escapes to the upper dressed state; consequently, a double-peak structure emerges in the PE spectrum. In the *lowest* frame of Fig. 8 (for $\theta = -\pi/2$), there is no (pronounced) avoided crossing at

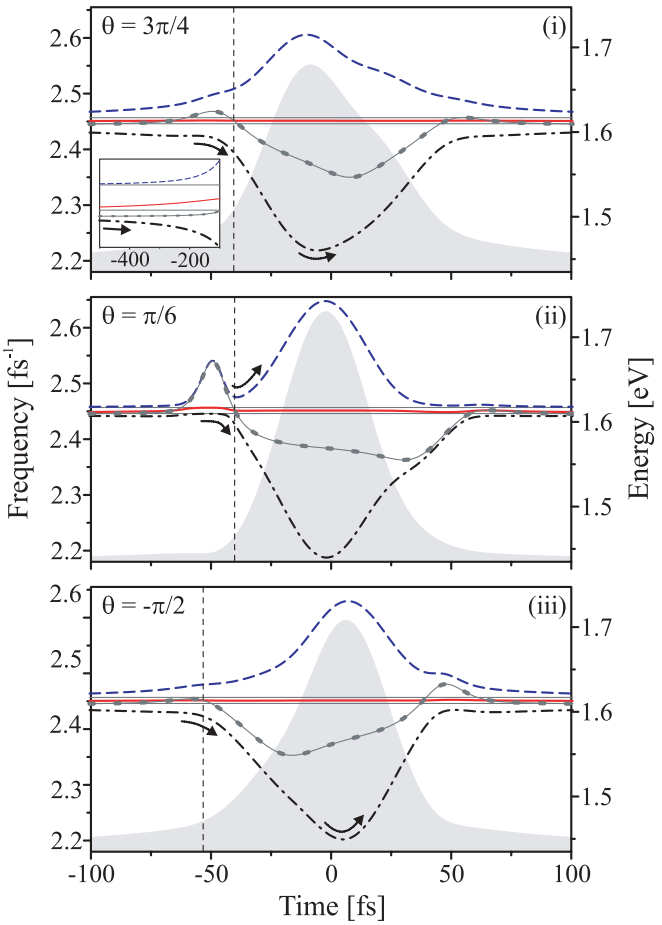


FIG. 8. (Color online) Time evolution of the dressed-state energies for a fixed position of the phase step $\omega_s = 2.443$ fs$^{-1}$ and for three values of the phase-step amplitude $\theta$: $3\pi/4$, $\pi/6$, and $-\pi/2$. The black dashed-dotted, the red solid, and the blue dashed curves show the dressed-state energies while the gray solid-dotted curve depicts the phase-step chirped energy of the (bare) state $|1\rangle$. The Rabi frequency is depicted as the gray shaded background. Arrows show the respective evolution path in each case, and the vertical dashed lines indicate the positions of the relevant induced avoided crossings.

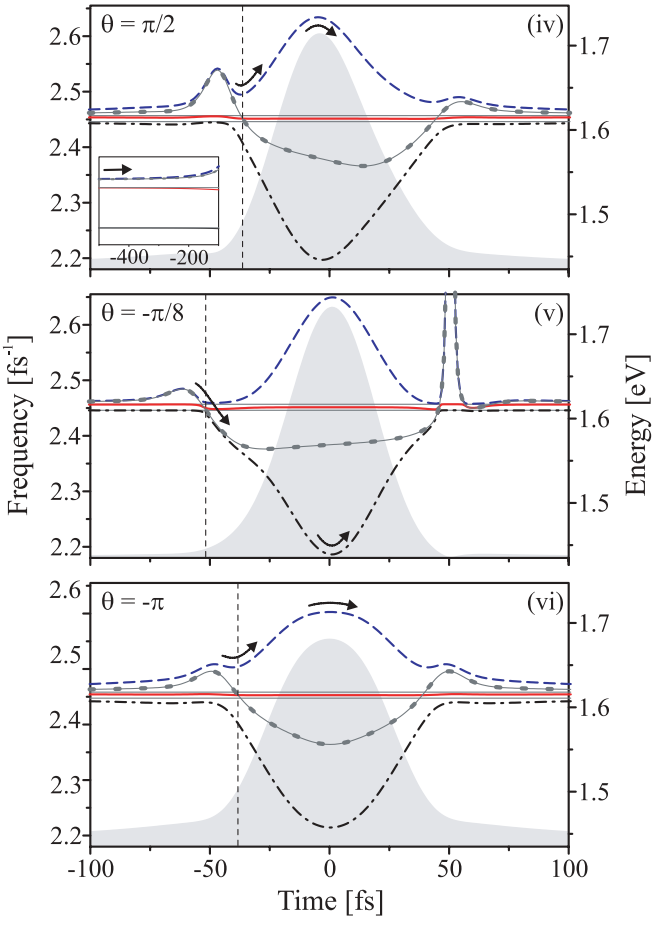


FIG. 9. (Color online) Time evolution of the dressed-state energies for a fixed phase-step position of $\omega_s = 2.459$ fs$^{-1}$ and for three values of the step amplitude $\theta = \pi/2$, $-\pi/8$, and $-\pi$. The notation is the same as in Fig. 8.

early times but only one around $t = +38$ fs, which is of no significance for the PE signal.

Figure 9 presents the dressed-state picture for a phase-step at $\omega_s = 2.459$ fs$^{-1}$, and for three values of the amplitude: (iv) $\theta = \pi/2$, (v) $\theta = -\pi/8$ and (vi) $\theta = -\pi$, which correspond to three high-signal islands in Fig. 7(b). For this value of $\omega_s$, it is the *highest* dressed state that is initially populated for $\theta = \pi$ (Fig. 5), which gives rise to the high-energy PE peak. As $\theta$ varies, avoided crossings emerge again in the dressed-state picture and they may change the course of the evolution. In the *upper* and *lower* frames of Fig. 9 the induced avoided crossings around $t = -36$ fs and $t = -38$ fs, respectively, are too broad and their presence is not of great significance because not much population escapes to the other dressed states: the population follows the highest dressed-state energy. In the *middle* frame of Fig. 9 (for $\theta = -\pi/8$), the avoided crossing occurs much earlier, around $t = -52$ fs, when the pulse amplitude is too weak to widen it. This crossing is therefore very narrow. Consequently, the evolution is diabatic there (it follows the solid-dotted curve) and most of the population escapes to the lowest dressed state; as a result, a low-energy peak is created in the PE spectrum around $\theta = -\pi/8$.

## V. CONCLUSION

In this contribution we studied coherent control of electronic excitation on a model system both experimentally and theoretically. Control was exerted by a *complex* shaped femtosecond laser pulse generated by a generalized spectral step-phase modulation function. In the experiment we studied PE spectra from a $1 + 2$ REMPI of potassium atoms, which served as a tool to map the dressed-state energy and population dynamics during the interaction. In addition to the common Autler-Townes doublet, a third dressed state was observed in the PE spectra. By using the suitable choice of both control parameters (i.e., the spectral phase-step amplitude $\theta$ and position $\omega_s$) we were able to switch among three distinct PE spectra each mapping selective population of one out of three dressed states. Our observations demonstrated the ability to switch the population among each of the three dressed states with high selectivity. Therefore, our experiments present a

generalization of earlier work toward SPODS in multilevel systems.

In the theoretical part, we presented a detailed analysis of the properties of the generalized spectral phase-step modulation relevant to understand the physical control mechanism in the time domain. Our study of the atomic excitation in terms of adiabatic dressed states revealed that the course of the evolution of the system, and hence the resulting PE signal, can be explained and predicted by analyzing the time evolution of multiple dressed-state energies. For adiabatic evolution conditions, as in the present experiment, the course of the evolution is established by identifying the induced avoided energy level crossings: a wide avoided crossing brings no transitions between the dressed states, whereas a narrow avoided crossing makes the system evolve diabatically and the population switches from one dressed state to another.

## ACKNOWLEDGMENTS

The Kassel group acknowledges financial support by the Deutsche Forschungsgemeinschaft (DFG). This work has also been supported by European Commission projects EMALI and FASTQUAST. Nikolay V. Vitanov acknowledges support by the Bulgarian Science Fund Grant Nos. VU-I-301/07, D002-90/08, and IRC-CoSiM.

[1] T. Baumert, J. Helbing, and G. Gerber, in *Advances in Chemical Physics*, edited by P. Gaspard and I. Burghardt (Wiley, New York, 1997).
[2] A. Assion *et al.*, Science **282**, 919 (1998).
[3] S. A. Rice and M. Zhao, *Optical Control of Molecular Dynamics* (Wiley, New York, 2000).
[4] M. Shapiro and P. Brumer, *Principles of the Quantum Control of Molecular Processes* (Wiley, New York, 2003).
[5] D. Tannor, *Introduction to Quantum Mechanics: A Time-Dependent Perspective* (University Science Books, Sausalito, CA, 2006).
[6] H. Rabitz, R. de Vievie-Riedle, M. Motzkus, and K. Kompa, Science **288**, 824 (2000).
[7] R. J. Levis and H. A. Rabitz, J. Phys. Chem. A **106**, 6427 (2002).
[8] M. Dantus and V. V. Lozovoy, Chem. Rev. **104**, 1813 (2004).
[9] M. Wollenhaupt, V. Engel, and T. Baumert, Annu. Rev. Phys. Chem. **56**, 25 (2005).
[10] T. Brixner *et al.*, in *Femtosecond Laser Spectroscopy*, edited by P. Hannaford (Springer, New York, 2005).
[11] J. Phys. B **41** *Special Issue on Coherent Control*, edited by H. Fielding, M. Shapiro, and T. Baumert (2008).
[12] H. Rabitz ed., New J. Phys. **11** *Focus on Quantum Control* (2009).
[13] E. T. Sleva, I. M. Xavier Jr., and A. H. Zewail, J. Opt. Soc. Am. B **3**, 483 (1985).
[14] Y. S. Bai, A. G. Yodh, and T. W. Mossberg, Phys. Rev. Lett. **55**, 1277 (1985).
[15] N. V. Vitanov, T. Halfmann, B. W. Shore, and K. Bergmann, Annu. Rev. Phys. Chem. **52**, 763 (2001).
[16] U. Gaubatz, P. Rudecki, S. Schiemann, and K. Bergmann, J. Chem. Phys. **92**, 5363 (1990).
[17] M. Wollenhaupt, A. Assion, O. Bazhan, C. Horn, D. Liese, C. Sarpe-Tudoran, M. Winter, and T. Baumert, Phys. Rev. A **68**, 015401 (2003).
[18] M. Wollenhaupt, A. Präkelt, C. Sarpe-Tudoran, D. Liese, T. Bayer, and T. Baumert, Phys. Rev. A **73**, 063409 (2006).
[19] M. Wollenhaupt, A. Präkelt, C. Sarpe-Tudoran, D. Liese, and T. Baumert, Appl. Phys. B **82**, 183 (2006).
[20] T. Bayer, M. Wollenhaupt, and T. Baumert, J. Phys. B **41**, 074007 (2008).
[21] M. Wollenhaupt, A. Präkelt, C. Sarpe-Tudoran, D. Liese, and T. Baumert, J. Opt. B **7**, S270 (2005).
[22] M. Wollenhaupt, D. Liese, A. Präkelt, C. Sarpe-Tudoran, and T. Baumert, Chem. Phys. Lett. **419**, 184 (2006).
[23] M. Wollenhaupt and T. Baumert, J. Photochem. Photobiol. A **180**, 248 (2006).
[24] T. Bayer, M. Wollenhaupt, C. Sarpe-Tudoran, and T. Baumert, Phys. Rev. Lett. **102**, 023004 (2009).
[25] M. Krug, T. Bayer, M. Wollenhaupt, C. Sarpe-Tudoran, T. Baumert, S. S. Ivanov, and N. V. Vitanov, New J. Phys. **11**, 105051 (2009).
[26] D. Meshulach and Y. Silberberg, Phys. Rev. A **60**, 1287 (1999).
[27] M. Renard, E. Hertz, B. Lavorel, and O. Faucher, Phys. Rev. A **69**, 043401 (2004).
[28] A. Präkelt, M. Wollenhaupt, C. Sarpe-Tudoran, and T. Baumert, Phys. Rev. A **70**, 063407 (2004).
[29] P. Panek and A. Becker, Phys. Rev. A **74**, 023408 (2006).
[30] A. Gandman, L. Chuntonov, L. Rybak, and Z. Amitay, Phys. Rev. A **75**, 031401(R) (2007).
[31] H. Suchowski, A. Natan, B. D. Bruner, and Y. Silberberg, J. Phys. B **41**, 074008 (2008).
[32] N. T. Form, B. J. Whitaker, and C. Meier, J. Phys. B **41**, 074011 (2008).
[33] B. Chatel, D. Bigourd, S. Weber, and B. Girard, J. Phys. B **41**, 074023 (2008).
[34] C. P. Koch, M. Ndong, and R. Kosloff, Faraday Discuss. **142**, 389 (2009).
[35] R. Bracewell, *The Fourier Transform and Its Applications* (McGraw-Hill, New York, 2000).
[36] M. Wollenhaupt *et al.*, in *Springer Handbook of Lasers and Optics*, edited by F. Träger (Springer, New York, 2007), Chap. 12.
[37] N. V. Vitanov, New J. Phys. **9**, 58 (2007).
[38] N. Dudovich, T. Polack, A. Pe'er, and Y. Silberberg, Phys. Rev. Lett. **94**, 083002 (2005).
[39] A. Weiner, Rev. Sci. Instrum. **71**, 1929 (2000).
[40] A. Präkelt, M. Wollenhaupt, A. Assion, C. Horn, C. Sarpe-Tudoran, M. Winter, and T. Baumert, Rev. Sci. Instrum. **74**, 4950 (2003).
[41] B. W. Shore, *The Theory of Coherent Atomic Excitation* (Wiley, New York, 1990), Vol. I.
[42] B. W. Shore, Acta Phys. Slov. **58**, 243 (2008).
[43] National Institute of Standards and Technology [http://www.nist.gov].
[44] J. R. Morris and B. W. Shore, Phys. Rev. A **27**, 906 (1983).